Supporting Information:

A Monolayer of Hexagonal Boron Nitride on Ir(111) as a Template for Cluster Superlattices

—

Supplementary information

Moritz Will,[*,†] Nicolae Atodiresei,[*,‡] Vasile Caciuc,[‡] Philipp Valerius,[†] Charlotte Herbig,[†] and Thomas Michely[†]

†*II. Physikalisches Institut, Universität zu Köln, Cologne, D-50937, Germany*

‡ *Peter Grünberg Institut (PGI-1) and Institute for Advanced Simulation (IAS-1), Forschungszentrum Jülich and JARA, Jülich, D-52425, Germany*

E-mail: will@ph2.uni-koeln.de; n.atodiresei@fz-juelich.de(theory)

Phone: +49 (0)221 470-6876

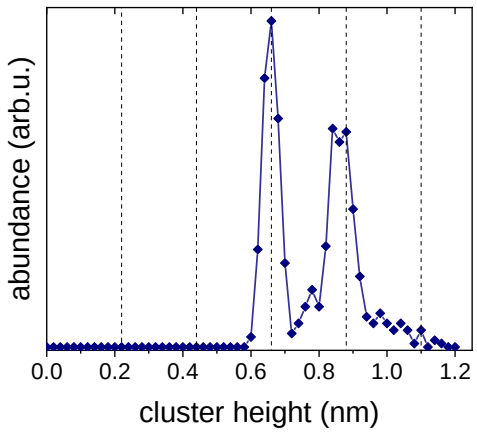

Figure S1: Cluster height distribution for the STM topograph shown in the main manuscript in Figure 1a, representing 0.57 ML Ir deposited at 250 K and imaged at 300 K. Dashed lines indicate integer multiples of the Ir(111) inter-layer distance 0.22 nm.

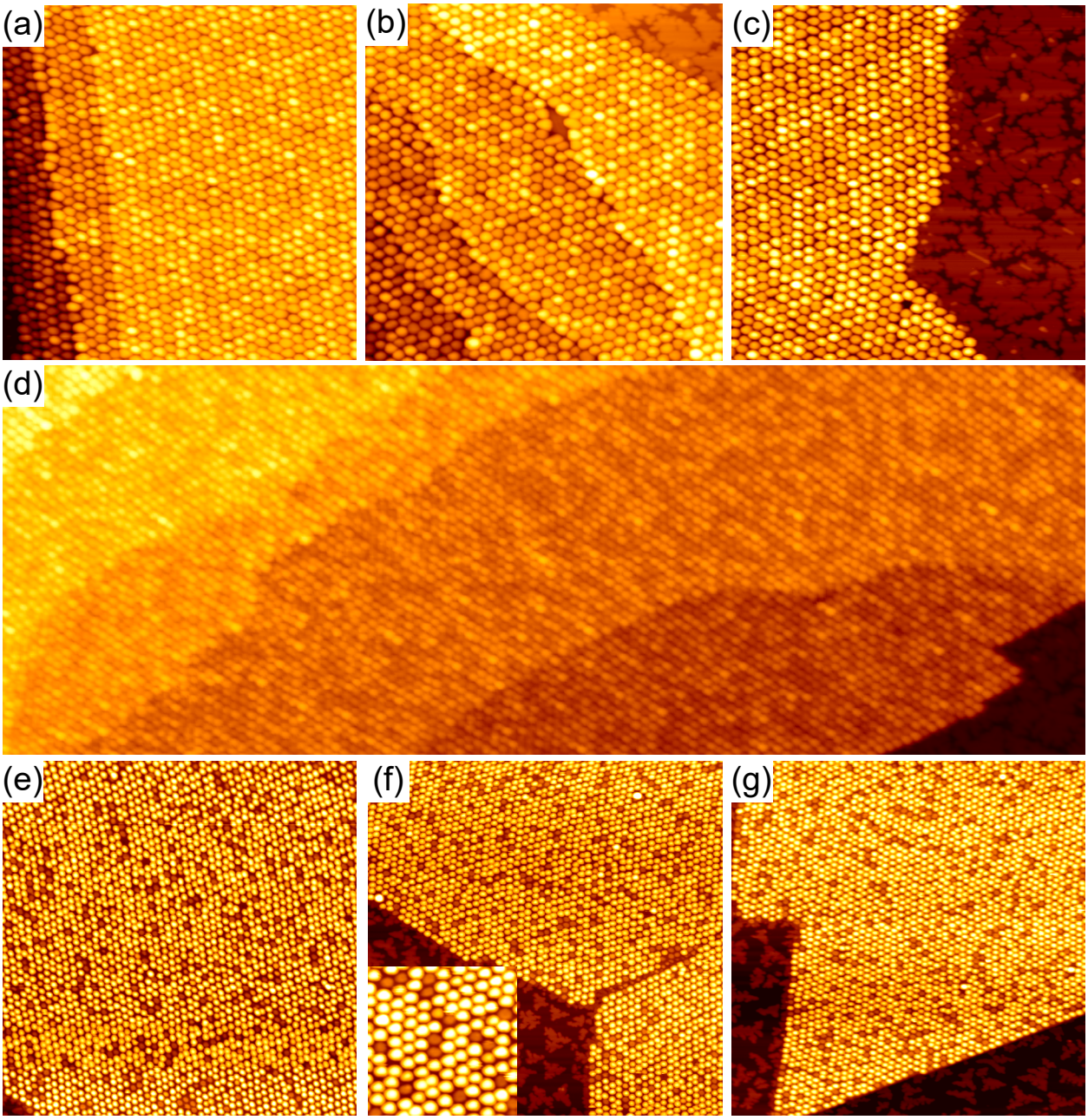

Figure S2: (a)-(d) STM topographs of 0.57 ML Ir deposited at 250 K and imaged at 300 K. (e)-(g) STM topographs of 0.34 ML Ir deposited at 350 K. The inset in (f) displays a magnified detail from the main image. Image sizes are (a)-(c) 80 nm × 80 nm, (d) 320 nm × 115 nm, (e)-(g) 133 nm × 133 nm, and for the inset in (f) 26 nm × 26 nm. Tunneling parameters are (a)-(c) $U_{bias} = -2.4$ V and $I_t = 58$ pA, (d) $U_{bias} = -2.7$ V and $I_t = 64$ pA, (e)-(g) $U_{bias} = -1.7$ V and $I_t = 59$ pA.

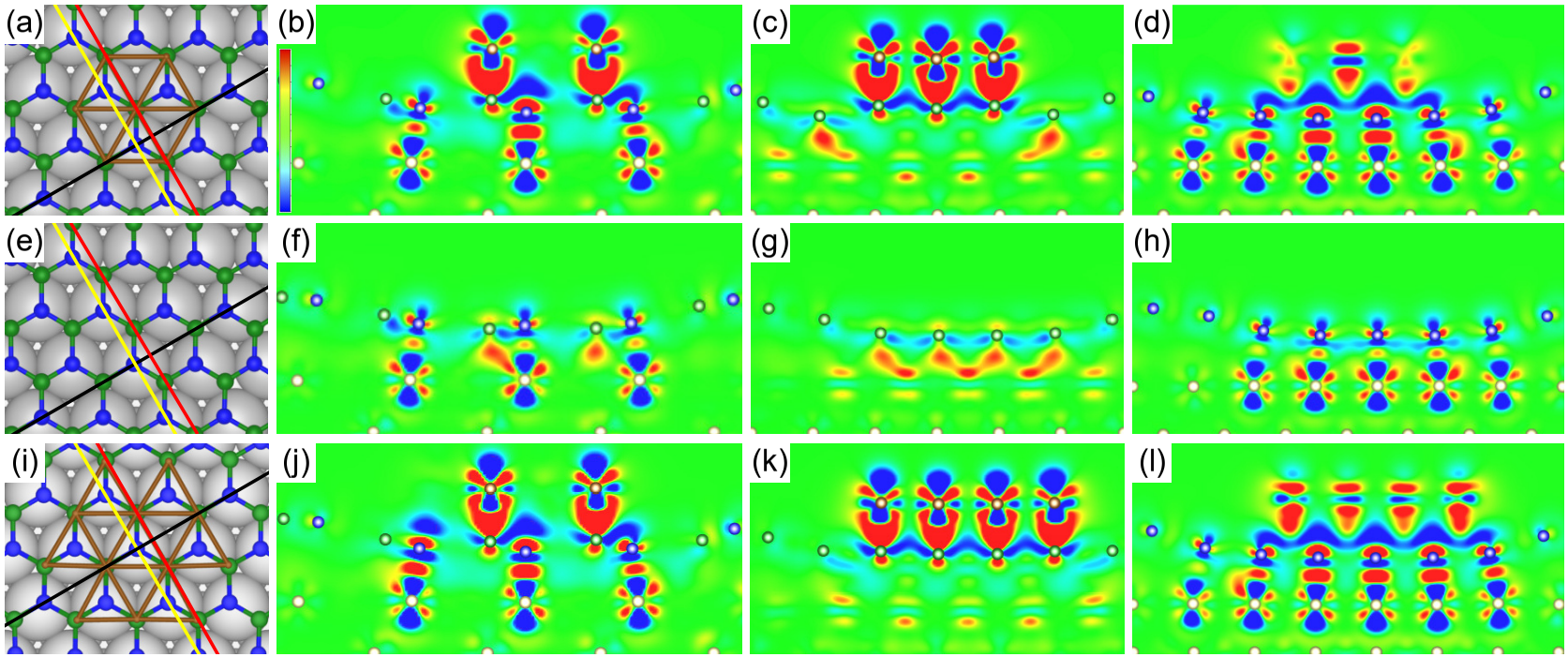

Figure S3: (a) Top view of a relaxed DFT geometry of an Ir heptamer (brown circles connected by sticks) adsorbed on h-BN on Ir(111). (b)-(d) Charge density difference between the relaxed system and subsystems of Ir cluster, h-BN and Ir substrate without changing atomic coordinates within each subsystem. The plot displayed in (b) is a cut along the black line in (a), (c) is along the red line, and (d) is along the yellow line. (e) Relaxed DFT geometry of the bare h-BN slab on Ir(111) without an adsorbed cluster. Correspondingly, (f) shows the charge density difference cut along the black line in (e), (g) along the red line and (h) along the yellow line. (i) Relaxed DFT geometry of an Ir dodecamer on h-BN on Ir(111). Again, (j) shows the charge density difference cut along the black line in (i), (k) along the red line, and (l) along the yellow line. In the geometries Ir substrate atoms are colored gray, B atoms green and N atoms blue. The color scale in the charge density difference plots ranges from a gain of $0.05\,\mathrm{e/A^3}$ (red) to a loss of $0.05\,\mathrm{e/A^3}$ (blue) in charge density.

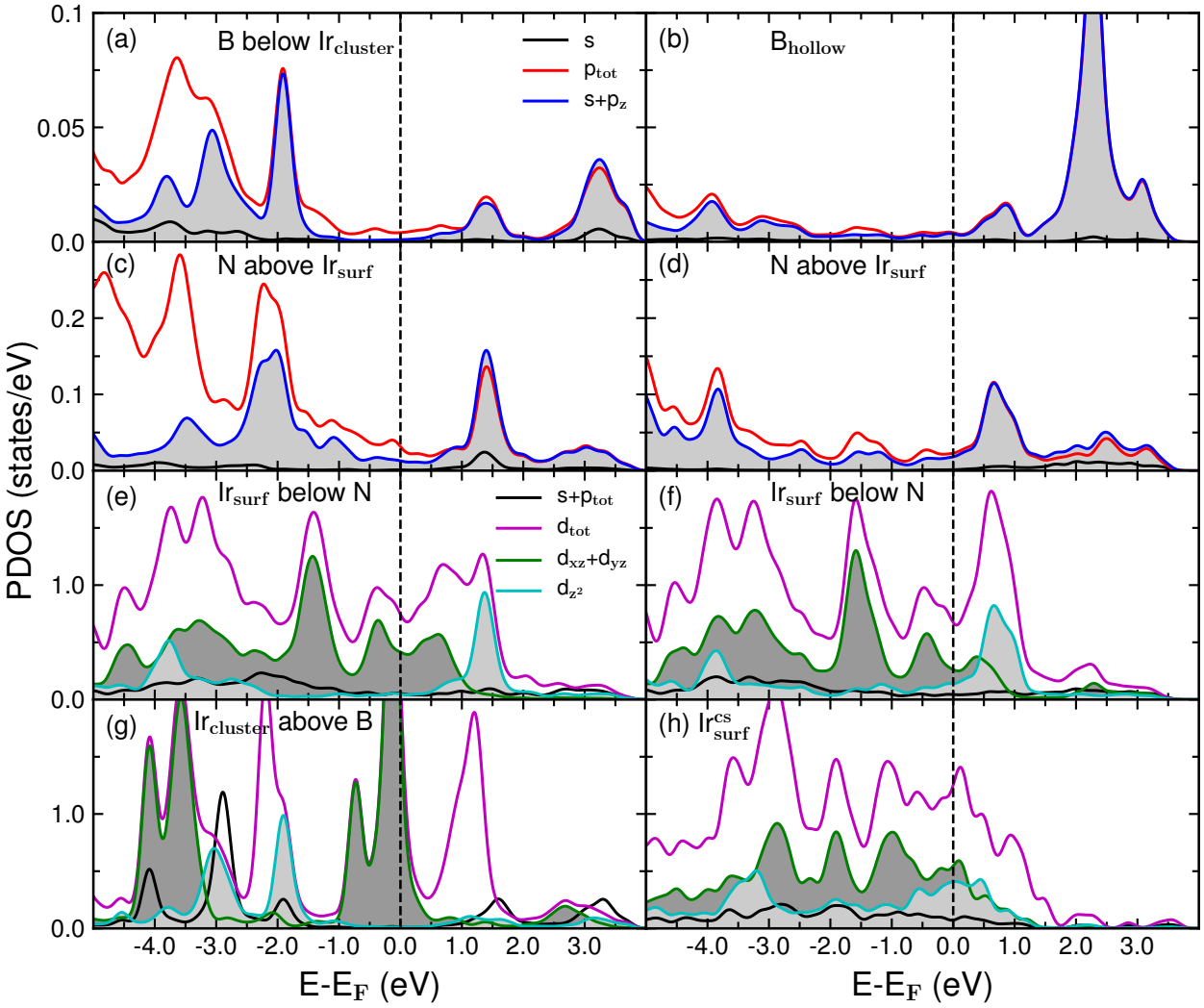

Figure S4: The projected density of states (PDOS) for (a) a B atom beneath an $Ir_{cluster}$ cluster atom, (b) the same B atom in a hollow site of the clean h-BN on Ir(111), (c) an N atom above an Ir_{surf} surface atom with adsorbed Ir cluster on top and (d) the same atom in the case of the pristine h-BN/Ir(111) system. Additionally, the PDOS of an Ir_{surf} atom below the N atom in the hybrid system (e) with and (f) without the Ir cluster as well as (g) that of an $Ir_{cluster}$ atom above the B atom are also shown. For comparison, in (h) the PDOS of the clean surface Ir^{cs}_{surf} atom with a substantial d_{z^2} contribution at E_F is depicted too. Then, as a key feature, note that at the Fermi energy E_F the electronic states of the h-BN on Ir(111) with and without the Ir cluster system are dominated by the out-of-plane $d_{xz} + d_{yz}$ states of the $Ir_{cluster}$ and Ir_{surf} atoms. On the other hand, the d_{z^2} orbitals of Ir_{surf} are split into bonding (below E_F) and anti-bonding (above E_F) states hybridized with the p_z ones of the N atoms located directly above them [see also Fig. 2(g) and (j) in the main text].

We note that the PDOS evaluated for a boron atom beneath an $Ir_{cluster}$ cluster one (see

Fig. S4a) exhibits a different peak structure as compared with the PDOS calculated for the same atom in a hollow site of the clean h-BN on Ir(111) (see Fig. S4b). This observation agrees well with a predominantly sp^3 hybridization of the h-BN in the valley region upon the adsorption of the Ir cluster while it is characterized by a sp^2 one in the case of the pristine h-BN/Ir(111) system.

Then, as discussed in the main text, the analysis of the PDOS for the Ir heptamer/h-BN/Ir(111) system revealed that at the h-BN/Ir(111) interface the surface Ir atoms form bonding and anti-bonding combinations with the p_z ones of the corresponding on-top N atoms (see Fig. S4c and e). A similar physical picture emerges for the clean h-BN on Ir(111) as depicted in Fig. S4d and f. However, the magnitude of this bonding-antibonding splitting of the Ir d_{z^2}- N p_z hybrid electronic states is significantly larger (by ≈ 0.8 eV) in the presence of the Ir cluster as compared to the clean h-BN/Ir(111) system, which clearly indicates a stronger local N-Ir interaction in the former case.

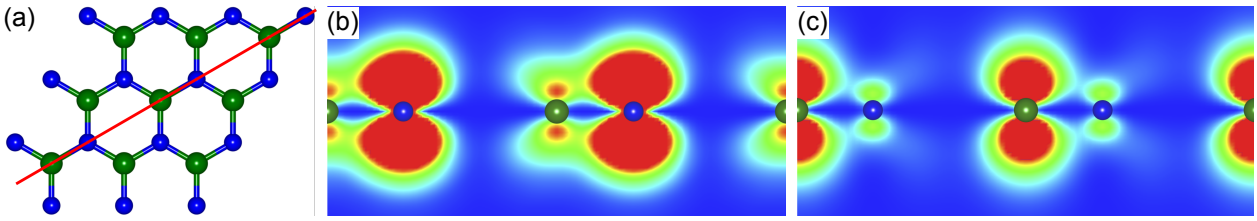

Figure S5: (a) Top view of a freestanding h-BN monolayer with a perpendicular plane crossing through the B-N bonds. (b) A charge density plot in the plane drawn in (a) for the highest occupied h-BN π-electronic states with a p_z character at the B and N atomic sites. Since N has a higher electronegativity as B, these π electronic states are mostly located at the N atoms with a large extension in space. (c) On the other hand, the lowest unoccupied π states of h-BN are predominantly located at the B atoms and exhibit also a substantial spatial extension.

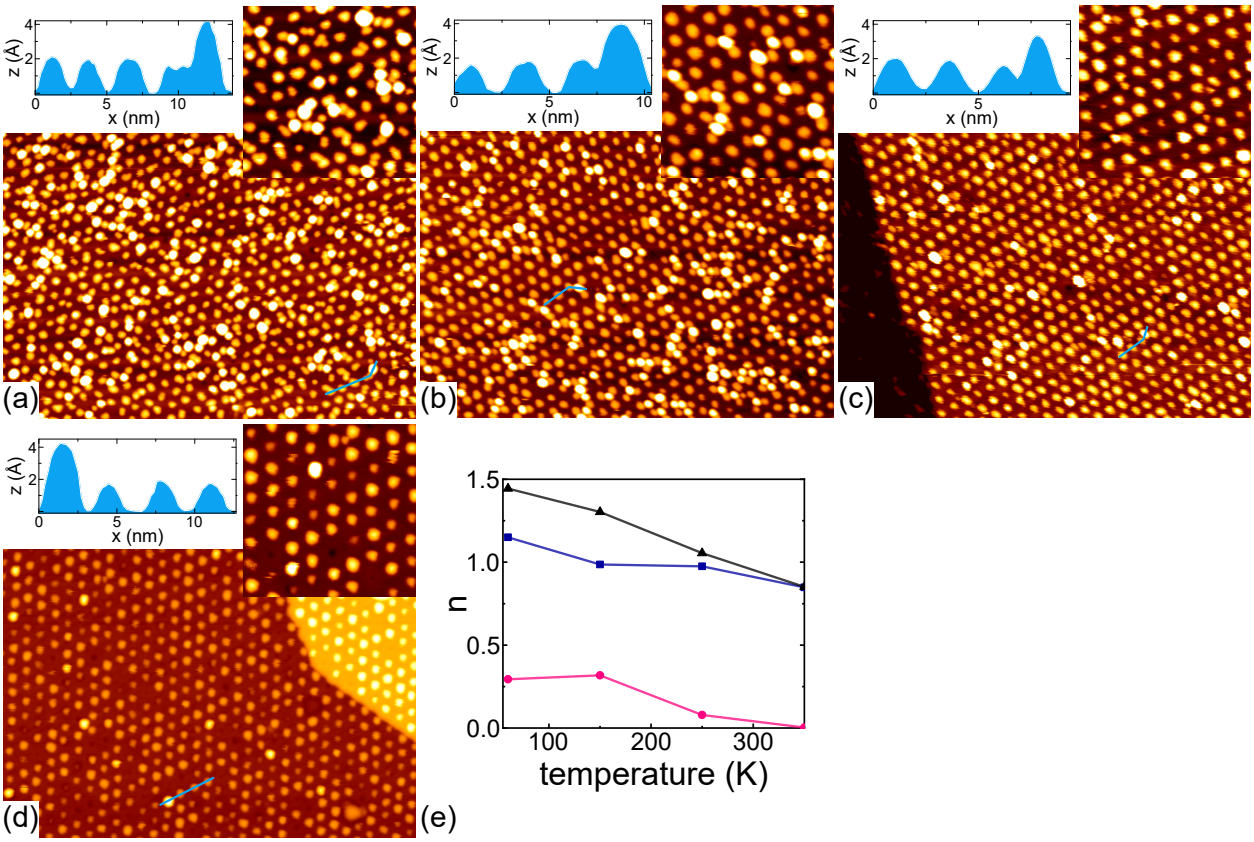

Figure S6: STM topographs of 0.05 ML Ir on h-BN/Ir(111), deposited at different temperatures. Deposition temperatures are: (a) 60 K, (b) 150 K, (c) 250 K, (d) 350 K. The image size is always 80 nm × 80 nm for the main images and 23 nm × 23 nm for the insets. All images were taken at temperatures lower than or equal to the indicated deposition temperature. (e) Cluster number density for the different deposition temperatures. Blue squares represent the number density of clusters in the valley n_{valley}, while pink dots are the cluster number density of center region clusters n_{center} (for the definition of the three regions in the moiré supercell, refer to Figure 2a in the main manuscript). Black triangles indicate the total cluster number density $n = n_{valley} + n_{center}$. Lines to guide the eye. Tunneling parameters are (a) $U_{bias} = -2.4$ V and $I_t = 84$ pA, (b) $U_{bias} = -2.4$ V and $I_t = 80$ pA, (c) $U_{bias} = -2.6$ V and $I_t = 50$ pA, (d) $U_{bias} = -2.9$ V and $I_t = 100$ pA.

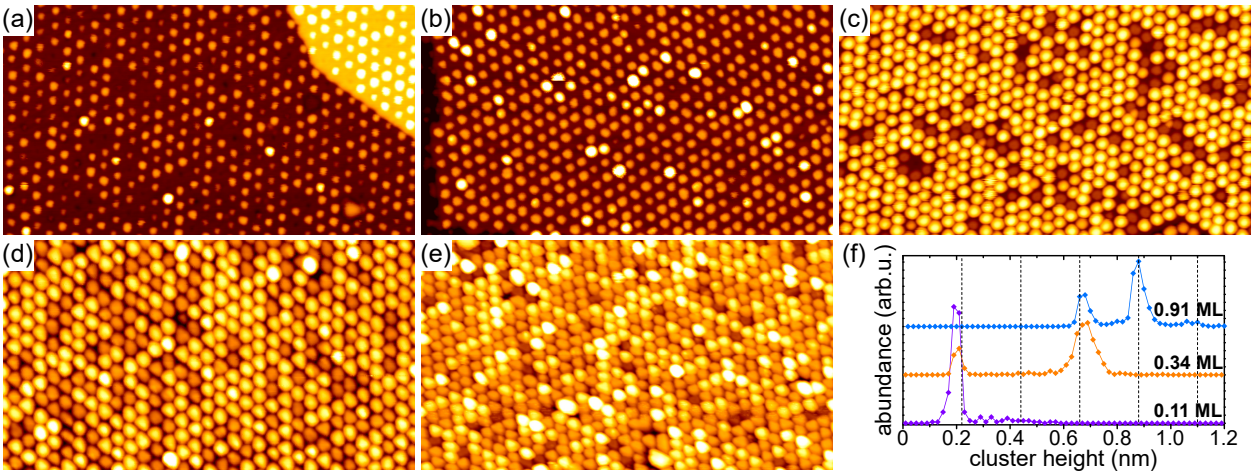

Figure S7: (a)–(e) STM topographs of h-BN/Ir(111) after deposition of an amount θ of Ir at 350 K. (a) $\theta = 0.05$ ML, average cluster size in atoms $s_{av} = 6$. (b) $\theta = 0.11$ ML, $s_{av} = 13$. (c) $\theta = 0.34$ ML, $s_{av} = 39$. (d) $\theta = 0.91$ ML, $s_{av} = 104$. (e) $\theta = 1.5$ ML, $s_{av} = 195$. The image size is always 80 nm $\times$ 45 nm. (f) Cluster height distribution for different coverages. Note that low cluster numbers are difficult to see in the distribution due to their fluctuating heights. This becomes apparent for two-layer clusters in the case of 0.11 ML and 0.34 ML Ir, or five-layer clusters for 0.91 ML Ir. Dashed lines indicate integer multiples of the Ir(111) inter-layer distance 0.22 nm. Tunneling parameters are (a) $U_{bias} = -2.9$ V and $I_t = 100$ pA, (b) $U_{bias} = -1.8$ V and $I_t = 65$ pA, (c) $U_{bias} = -1.7$ V and $I_t = 59$ pA, (d) $U_{bias} = -1.6$ V and $I_t = 64$ pA, (e) $U_{bias} = -1.7$ V and $I_t = 140$ pA.